J Mater Sci (2012) 47:779–792
DOI 10.1007/s10853-011-5854-4

On the development of microstructures and residual stresses during laser cladding and post-heat treatments

Jianyin Chen · Sheng-Hui Wang · Lijue Xue

Received: 3 May 2011 / Accepted: 4 August 2011 / Published online: 19 August 2011

Abstract In this article, laser cladding process with a blown powder feeding was used to deposit nickel-based IN-625 superalloy, cobalt-based hardfacing Stellite 6 alloy and high-vanadium CPM 10V tool steel onto a similar or dissimilar base material, respectively, to investigate the development and controllability of process-induced residual stresses in the clad and to analyse their correlation with microstructural evolutions of the clad and heat-affected zone (HAZ) during cladding and post-heat treatments. The residual stresses were evaluated using the hole-drilling method as per ASTM E837-95, whereas the microstructures were studied using X-ray diffractometer, optical microscope and scanning electron microscope. A particular attention was paid to combined effect of both clad and HAZ on the build-up of residual stresses in the clad. It is expected that the experimental results will form a useful addition to the existing knowledge with respect to the topic and, more significantly, to promote confidence on industrial applications of laser-clad IN-625, Stellite 6 and CPM 10V materials.

Introduction

Laser cladding process by blown powder feeding can deposit a layer of material onto the surface of a similar or a dissimilar base material (or substrate) to produce metallurgically sound and dense clad [1–4]. In the most recent 20 years, many industrial applications have been reported, the majority of which can be found in two fields: (1) laser cladding to deposit high-performance material onto a surface of different base material (such as a component, part, tool, mould, die, or others) to enhance the functional properties of the surface, such as the resistance against corrosion, wear, or high-temperature oxidation; and (2) laser cladding (or laser cladding based freeform fabrication) to repair/restore original geometries and functionalities of a damaged base material and, sometimes, to recover a undersized expensive material due to machining or grinding errors [2–6]. Although other alternative processes, such as TIG welding, thermal spraying, gas dynamic spraying (GDS), e-beam deposition and others [7–12], are available for the similar tasks, laser cladding presents some unique advantages, considering various factors relevant to overall costs of materials, equipment and manufacturing processes as well as the quality of deposited materials. For instance, laser cladding uses a relatively low heat input to produce a clad with metallurgical bonding to the substrate, lessening the distortion of the substrate and minimizing the dilution of cladding material into the substrate which, consequently, reduces undesired deterioration of properties of the substrate.

In spite of a relatively low heat input, a small portion of base material (or substrate) along with cladding material still has to be melted by a moving laser beam and re-solidified to form a clad track during cladding, which could introduce certain amount of residual stresses and distortion in the clad and substrate, especially when a relatively large area is deposited. In some cases, the presence of residual stresses might cause cracking or even delamination. In addition, residual stresses play an important role in the mechanical behaviours (such as fatigue, creep and

J. Chen (✉) · L. Xue
Industrial Materials Institute, National Research Council of Canada, 800 Collip Circle, London, ON N6G 4X8, Canada
e-mail: jianyin.chen@nrc.gc.ca

S.-H. Wang
Chalk River Laboratories, Atomic Energy of Canada Limited, Chalk River, ON K0J 1J0, Canada

brittle fracture properties) of laser-clad materials. Normally, the presence of tensile stresses at the surface of a clad material could result in its premature failure, whereas the existence of compressive stresses at the surface of the clad material could improve its service life. Nevertheless, residual stresses could be effectively controlled, for instance, by optimizing laser process parameters (heat input) and deposition strategy, by depositing an interlayer or graded transition layer between the clad and the substrate to compensate their thermal mismatch, by preheating the substrate to reduce the thermal mismatch or retard solid-state phase transformations, or by performing stress-relieving treatment and so on [13–17].

It is well known that the development of residual stresses in a laser-clad is a complex process which depends not only on thermal effects generated by laser beam (process parameters) but also on temperature-dependent physical and mechanical responses of the material being involved [13, 14]. A number of representative reviews and researches [13, 14, 18–27] on the development of residual stresses in welding/cladding are available in public domain. Inoue [18, 19], for example, proposed a generic metallo-thermo-mechanical interactive model for thermal processes such as welding (applicable to laser cladding), continuous casting and quenching: a change of temperature distribution in a body would introduce thermo-mechanical effect (thermal stress) and/or temperature-dependent phase transformation effect (transformation stress and transformation plasticity), which would generate residual stresses in the concerned body. Meanwhile, deformation-induced heat and phase transformation generated latent heat would, in return, disturb the existing temperature field in the same body, and the presence of stress/strain in the same body might induce phase transformation effect as well. Therefore, during the study of the development of residual stresses in a specific laser-clad, these relationships should be kept in mind, with a focus on possible dominant contributors (as, for instance, suggested by Pilloz's model [20]) by ignoring insignificant factors. It is reasonable to assume that the laser-clad and the underlying heat-affected zone (HAZ) are stress-free at solidification temperature of the clad due to their low yield strengths at this point of the time. Therefore, it is the material behaviours in both solidified clad and HAZ, during the stage of cooling after solidification of the melt (cladding material), that determine the resulting stress state in the clad [20, 21].

In this article, nickel-based IN-625 superalloy, cobalt-based hardfacing Stellite 6 alloy and Crucible's CPM 10V tool steel (containing a large amount of vanadium carbides) were selected as cladding materials for the study of process-induced residual stresses since those alloys are used in either manufacturing/repairing high-value aerospace components/parts (such as IN-625 [28]) or enhancing surface performance of components, parts, tools, dies or moulds (such as Stellite 6 [29, 30] and CPM 10V [31, 32]). To deal with the complicated issue in a simple way, this study would be focused on thermo-mechanical and phase transformation effects during cooling, as proposed by Refs. [20, 21], for investigating the development and controllability of residual stresses in a clad and its correlation with microstructural evolution of the clad and HAZ. The experimental results could be a useful addition to the existing knowledge with respect to the topic, enlarging the database regarding laser processing and, more significantly, promoting confidence on industrial applications of laser-clad IN-625, Stellite 6 and CPM 10V materials.

Experimental

Cladding and substrate materials

The commercial nickel-based IN-625 (Praxair Surface Technologies, Inc., Indianapolis, IN), cobalt-based hardfacing Stellite 6 (Deloro Stellite Inc., Belleville, ON) and high-vanadium CPM 10V (Crucible Research Center, Pittsburgh, PA) powders were used as cladding materials. The gas-atomized powders of IN-625, Stellite 6 and CPM 10V were spherical in shape with a size range of 15–45 μm in diameter. Wrought IN-625 alloy plate, ASTM Class "C" wheel steel plate and AISI 1070 carbon steel plate in "as-received (i.e., annealed)" condition, on the other hand, were used as base materials (or substrates). Both chemical compositions of the cladding materials (as provided by the respective suppliers) and the nominal chemical compositions of the substrate materials [33–35] were summarized in Table 1. Prior to cladding, the surfaces of the substrates were ground and degreased with acetone to maintain the consistent energy absorption of the laser beam.

Laser cladding process

The laser cladding process with injecting powder feedstock, illustrated in Fig. 1a, was used. The experimental setup employed a 3 kW continuous wave (CW) CO_2 laser (model: GE Fanuc C3000), a precision powder feeder (model: Mark XV-RC) and a computer numerically controlled (CNC) motion system. Both laser focusing optics and powder feeding nozzle were mounted on the z-axis of the CNC motion system while a substrate was clamped on the x–y motion table. Laser cladding was carried out in a glove box filled with argon to maintain an oxygen level below 50 ppm. In addition, argon was also used as carrying gas for the delivery of the powder and as shielding gas for the laser optics during the process.

Table 1 Chemical compositions of cladding and substrate materials (wt.%)

Chemical element	IN-625 powder	Wrought IN-625 [33]	Stellite 6 powder	ASTM Class "C" wheel steel [34]	CPM 10V powder	AISI 1070 steel [35]
Chromium	22.0	21.5	27.0	<0.25	5.25	
Molybdenum	9.0	9.0		<0.10	1.30	
Tungsten			4.7			
Manganese			<0.1	0.60–0.90	0.50	0.60–0.90
Silicon			0.9	0.15–1.0	0.90	0.15–0.30
Vanadium				<0.04	9.75	
Niobium		3.6		<0.05		
Tantalum (+Niobium)	3.7					
Carbon	0.03	0.05	1.0	0.67–0.77	2.45	0.65–0.75
Copper				<0.35		
Aluminium		0.2		<0.06		
Titanium		0.2		<0.30		
Nickel	Bal.	Bal.	<0.1	<0.25		
Sulphur				0.005–0.040		<0.050
Phosphorous				<0.03		<0.040
Cobalt			Bal.			
Iron	0.4	2.5	0.7	Bal.	Bal.	Bal.

During laser cladding, a 190 mm focal length lens was used to focus the laser beam onto a substrate to create a melt pool ($\sim$3.0 mm) where the metallic powders were injected. With a traversing movement, the melt pool was travelling along, leaving a clad track (solidified "melt pools") that was metallurgically bonded to the substrate. By re-melting a portion of the preceding clad track and the substrate, the second clad track was deposited neighbouring to the first one, with a normal overlap of 30–35%. Repeatedly, the first layer of the clad was formed by depositing multiple clad tracks with partial overlap. Subsequent layers can be further deposited onto the previous layers, until the desired clad thickness was achieved. After cladding, the clad specimens so obtained were ground to flatten their surfaces, and the final dimensions of the specimens were summarized in Table 2. The laser-clad IN-625 plates used for the current study were demonstrated in Fig. 1b.

It should be noted that, for laser cladding of hardened materials such as CPM 10V tool steel, cracking might appear in the clad as a result of build-up of process-induced stresses. In order to improve the cladability of CPM 10V steel, an "on-site" pre-heating of the substrate (150–200 °C) was used to alleviate the accumulation of the stresses and to prevent cracking or delamination during cladding.

Post-cladding heat treatments

In order to investigate the effectiveness of stress-relieving on laser-clad IN-625, Stellite 6 and CPM 10V materials, various post-cladding heat treatments (annealing or tempering) were applied on the clad specimens (Table 3). The selected temperature for a specific clad specimen should prevent significant degradation of mechanical properties of the respective base material (or substrate).

Materials characterization

The laser-clad specimens were mechanically cross-sectioned, ground, polished and chemically etched for the metallographic study. The morphology of the clad was revealed using an Olympus optical microscope (OM); while the microstructure was studied using a Hitachi S-3500 variable pressure scanning electron microscope (VP-SEM) along with an Oxford energy dispersive spectrometer (EDS). The phases presented in the clad were identified using a Philips X'Pert X-ray diffractometer (XRD) with a graphite-monochromatic CuK_α radiation ($\lambda = \sim 1.54$ Å).

The hardness of clad specimens was measured using a NewAge's Rockwell hardness testing system. Any hardness data reported here were statistic averages of at least five measurements. The microhardness profiles across the thickness of clad and substrate were measured on a Buehler's microhardness tester using a Vickers indentor.

Stress analysis

The hole-drilling strain gage method as per ASTM E837-95 was used to determine residual stresses in a clad. The measurements were conducted by using an RS-200 milling

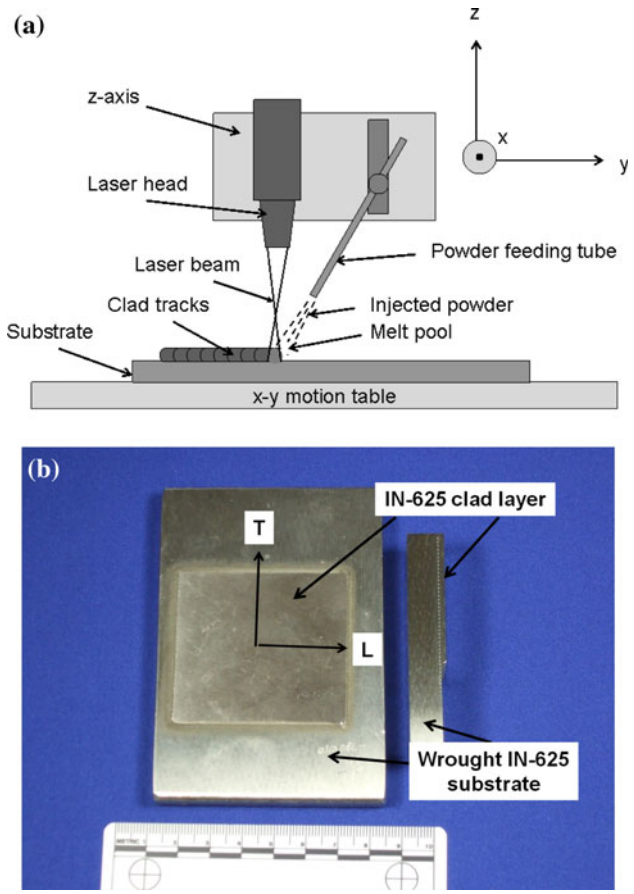

Fig. 1 **a** An illustration of laser cladding process by blown powder feeding and **b** laser-clad IN-625 alloy on wrought IN-625 substrate, where the "L" and "T" represent the direction parallel to and transverse to the laser cladding path, respectively

guide and a strain measurement system (Measurement Group, Inc., Raleigh, NC). A special strain gage rosette (type: TEA-06-062RK-120) was glued on the clad surface at the centre of the clad specimen where the relieved strains were to be measured. A high-speed air turbine mill with a carbide cutter was used to drill a flat-bottom hole (with a depth of about 0.6 mm) at the centre of the strain gage rosette, while the relieved strains in the vicinity of the hole were measured by the strain gage. The stresses were then deduced using ReStress® software supplied with the system, where the moduli of the laser-clad IN-625, Stellite 6 and CPM 10V materials were 207 GPa [36], 209 GPa [29] and 234 GPa [37], respectively. The stresses thus obtained reflected the local average values in the clad across a depth of about 0.6 mm from the clad surface. Nevertheless, even though the actual residual stresses were non-uniform through the thickness of the clad, the measured values still reflected the nature of the process-induced stresses in the clad. It should be noted that the measurement errors might be introduced during the installation and alignment of strain gage and milling guide, and during the hole drilling [38]. In a normal case, the usual precision of measured stress obtained using the hole-drilling method is ±20 MPa [39].

Results and discussion

The process parameters for laser cladding of all three cladding materials in this article have been reasonably optimized to produce metallurgically sound and dense clads with no crack and very few pores. Since the microstructural evolution of the clad and the HAZ of the substrate may contribute significantly to the development of stresses in the clad both during cladding and during post-cladding heat treatments, metallurgical examination of the clad specimens was focused on process-induced microstructural characteristics of the clad and the HAZ as well as on their combined effects on the development of stresses in the clad.

Table 2 The dimensions of clad specimens (where the length and width of the clad are parallel to and transverse to the laser cladding direction, respectively)

Clad specimen (clad/substrate)	Clad size (mm) (approximation)	Number of layers	Substrate size (mm) (approximation)
IN-625/IN-625	55 (long) × 50 (wide) × 2.0 (thick)	3	105 (long) × 75 (wide) × 10.0 (thick)
Stellite 6/Class "C"	45 (long) × 35 (wide) × 2.5 (thick)	5	80 (long) × 65 (wide) × 12.5 (thick)
CPM 10V/1070	55 (long) × 35 (wide) × 2.0 (thick)	2	85 (long) × 60 (wide) × 12.5 (thick)

Table 3 Post-cladding heat treatments for various laser-clad materials

Clad specimen	Post-cladding heat treatment
IN-625/IN-625	760 °C (1400°F), 816 °C (1500°F) and 871 °C (1600°F) for 1 h, air cooling
Stellite 6/Class "C"	500, 600, 650 and 700 °C for 2 h, furnace cooling
CPM 10V/1070	260 and 600 °C for 2 h, furnace cooling

In terms of mechanism of the development of residual stresses in a laser-clad, Pilloz et al. [20] had suggested a straightforward phenomenological approach (that is, three blocks model based on a decomposition of the clad specimen into three parts: clad, HAZ and unaffected substrate) to semi-quantitatively evaluate the magnitudes and signs of residual stresses. Although experimental results have shown that residual stress fields formed inside the laser-clad and the surrounding area were far more complicated [26], the proposed approach [20] could still reasonably qualitatively (albeit not quantitatively) estimate the development of residual stresses in the laser-clad. Accordingly, for the purpose of assessment of residual stresses, a clad specimen in this study, was simply considered to have three major layers (or blocks) through its thickness: the clad, the HAZ (which corresponds to the portion of the substrate significantly affected by thermal cycles during cladding) and the unaffected substrate (where thermal effect of cladding process is negligible). It was expected that each of the three layers would demonstrate different thermo-metallo-mechanical behaviours in the development of residual stresses during cladding and post-cladding heat treatments [20, 21].

Laser-clad IN-625 superalloy onto wrought IN-625 superalloy

Figure 2a shows the microstructures across the interface between IN-625 clad and wrought IN-625 substrate, where the "as-clad" microstructure can be characterized as refined dendrites with different orientation, whereas the substrate shows equiaxed grains. The HAZ (IN-625), which is referred to the zone just beneath the IN-625 clad layer, was difficult to be differentiated from the rest of substrate under an optical microscope. After annealing at 760 °C (1400°F), 816 °C (1500°F) and 871 °C (1600°F) for 1 h, respectively, the dendrites in the clad and the grain structures over the substrate still remained intact, as illustrated in Fig. 2b for the case of the clad specimen annealed at 871 °C for 1 h. Further X-ray diffraction analysis revealed that the major phase presented in the IN-625 clad in both "as-clad" and "after annealed at 871 °C for 1 h" conditions was a single γ phase with f.c.c. structure.

Figure 3 depicts the depth profiles of microhardness of the laser-clad IN-625 in both "as-clad" and "after annealed at 871 °C for 1 h" conditions, where a solid line marked the interface between the clad and the substrate before cladding. After cladding, a mixture of the cladding material and the substrate has created a layer with compositional dilution (a zone bounded by the solid and dashed line in Fig. 3). Measured with an optical microscope, the diluted layer was about 0.5 mm thick. The average microhardness in the clad and entire substrate shows no substantial difference in both "as-clad" and "after annealed" conditions.

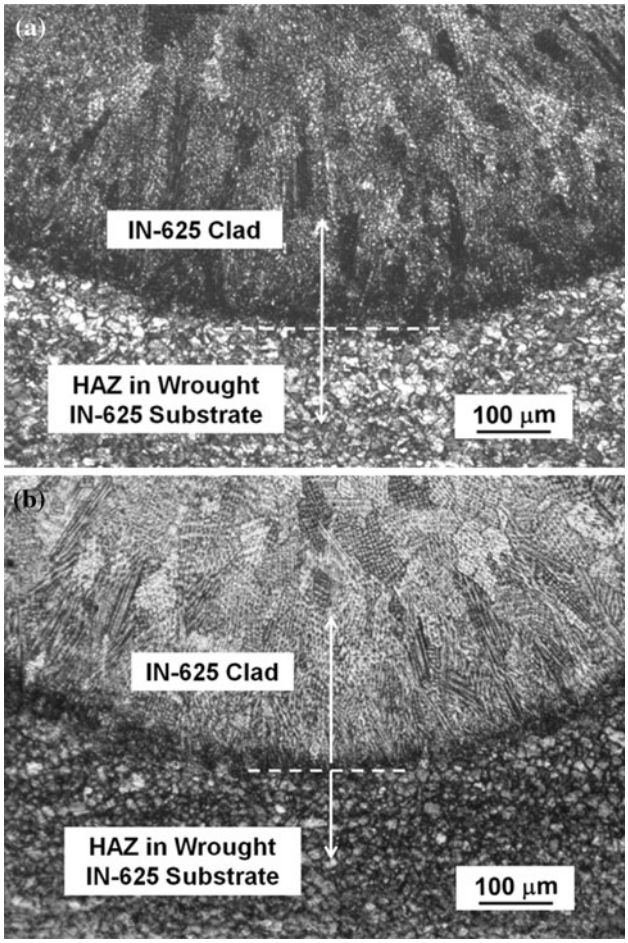

Fig. 2 Optical microstructures of laser-clad IN-625 on wrought IN-625 **a** in "as-clad" condition and **b** in "after annealed at 871 °C for 1 h" condition

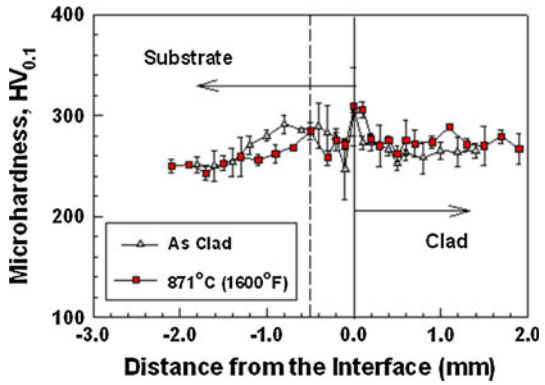

Fig. 3 Depth profiles of microhardness of laser-clad IN-625 on IN-625 in "as-clad" and "after annealed at 871 °C for 1 h" conditions

Figure 4 shows the influence of annealing process on residual stresses and hardness of the IN-625 clad. The "as-clad" IN-625 shows biaxial tensile stresses, σ_L and σ_T in the clad being about 387 and 265 MPa, respectively, where the "L" and "T" represent the direction parallel and

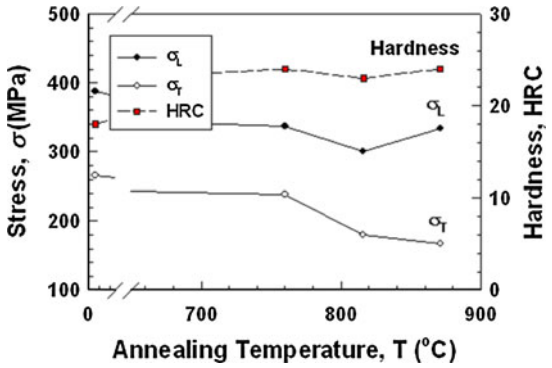

Fig. 4 The residual stress (σ) and hardness in IN-625 clad versus annealing temperature, in which the "L" and "T" represent the stress parallel to and transverse to the laser cladding direction, respectively

transverse to the laser deposition path. It should be pointed out that: (1) the σ_L was higher than the σ_T, in "as-clad" condition and the same trend was remained after various post-cladding annealing; and (2) the directions of the σ_L and σ_T were not always the principal stress axes, which could have a tilt angle with the laser cladding direction. The direction-dependent distribution of residual stresses is an issue of the complexity, and has something to do with laser process parameters (such as overlap percentage of neighbouring laser-clad tracks, height of the clad and laser scanning speed) [26] and/or boundary constrains on the clad [13, 14]. De Oliveira et al. [26] found, after investigating residual stresses of Co-based laser-clad, that the major principal stress axis tends to lie perpendicular to the solidification front; when a single clad track is deposited, a solidification front on the surface moves with the laser scanning direction and the major stress axis is expected to lie along the cladding direction; a partial overlap of the neighbouring clad tracks could change the direction of the solidification front, and create a tilt angle toward the laser cladding direction, which, thereafter, causes a misorientation between the principal stress axis and laser cladding direction. For the current cases, with the presence of the tilt angles, all the measured stresses were transformed into the directions along and transverse to the laser cladding path for the convenience of discussion.

Annealing has reduced the magnitudes of stresses in the clad to certain degree. For example, after annealing at 760 °C for 1 h, the biaxial stresses (σ_L and σ_T) in the IN-625 clad experienced a reduction of 10–13% in their magnitudes, reaching 337 and 239 MPa, respectively, and they have been lowered down to about 334 and 167 MPa, respectively, after annealing at 871 °C for 1 h.

Since the clad and the substrate were identical, there was no difference in coefficient of thermal expansion (CTE) between them, and thermal deformation was solely a function of temperature. It was reasonably assumed that the solidified clad and the HAZ experienced similar temperatures during continued cooling; it was further assumed that, at the time when solidification of the clad completed, no stress existed in the underlying HAZ since, based on the fact that the temperature at the HAZ during heating was high enough to reach that point for relieving and nullifying any potential stresses (e.g., possible compressive stresses due to thermal expansion constrained by the substrate) by thermal relaxation. For the same reason, it was simply assumed that the clad, the HAZ and the unaffected substrate all had the equivalent length (Fig. 5a) and were stress-free at this point of the time. During subsequent cooling, both clad and HAZ experienced a simultaneous thermal contraction (Fig. 5b), while constrained by the unaffected substrate (with an unchanged length), generating internal tensile stresses. The tensile stresses in the clad and HAZ would be balanced by compressive stresses in the unaffected substrate. Since no solid-state phase transformation occurred in both clad and HAZ during the period of cooling, the tensile stresses in them would be retained at ambient temperature. Conlon et al. [40], in collaboration with the authors, have experimentally confirmed the presence of such kind of through-thickness profiles of residual stresses in the laser-clad IN-625 using neutron diffraction method.

During subsequent annealing, since no solid-state phase transformation occurred in both clad and substrate, the dominated mechanism was stress relaxation at high temperature, where the yield strength of the material was significantly decreased (for example, the yield strength ($\sigma_{0.2}$) of wrought IN-625 alloy at 25, 760 and 870 °C was

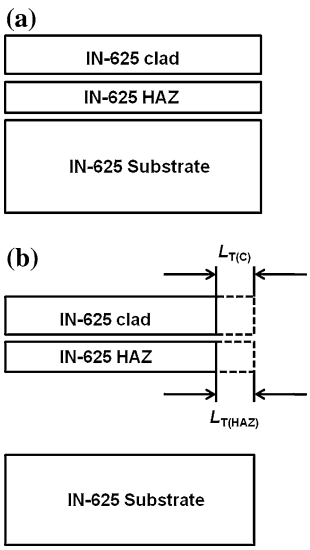

Fig. 5 Schematic of overall deformations (L) of the IN-625 clad, the HAZ and the unaffected substrate during cooling, if not impeded: **a** at solidification temperature of the clad and **b** at ambient temperature, where the subscript "T" refers to thermal-induced, whereas the subscripts "C" and "HAZ" represent clad and heat-affected zone, respectively

about 490, 345 and 205 MPa, respectively [41]). As a result, it was easy for both clad and substrate to minimize their difference in the process-induced distortion through high-temperature creep, which consequently reduced the magnitudes of stresses in the clad. As a general rule, the higher the annealing temperature, the less the residual stresses retain (Fig. 4).

Laser-clad Stellite 6 onto ASTM Class "C" wheel steel

Figure 6a shows the microstructures of "as-clad" Stellite 6 alloy and HAZ (in Class "C" wheel steel substrate). The Stellite 6 clad was composed of a refined hypoeutectic structure containing primary dendrites (cobalt-based solid solution, α) and interdendritic eutectics (a combination of laminar M_7C_3 and α, where M = Cr, Co, W). This observation was similar to the one reported in Refs. [42, 43]. The HAZ (about 0.9 mm thick) exhibits martensitic characteristics (Fig. 6a), in contrast to its originally annealed microstructure, indicating that the HAZ has been re-austenitized and self-quenched during cladding. Furthermore, after annealing at 500, 600, 650 and 700 °C for 2 h, respectively, the dendritic structure in the clad still remained intact, but the martensitic HAZ has been gradually restored to near equilibrium phases (Fig. 6b).

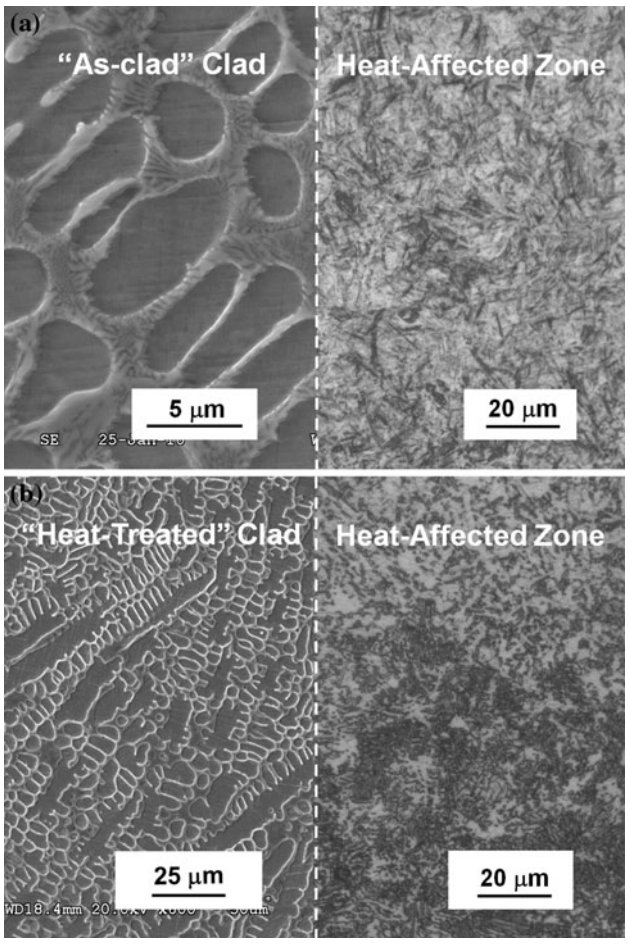

Fig. 6 Microstructures of laser-clad Stellite 6 on ASTM Class "C" wheel steel substrate: **a** in "as-clad" condition and **b** "after annealed at 700 °C for 2 h" condition

Figure 7 shows the depth profiles of microhardness of the laser-clad Stellite 6 in both "as-clad" and "after annealed at 700 °C for 2 h" conditions. The penetration (or dilution) layer was about 0.3 mm thick. In "as-clad" condition, the average microhardness of the clad, the HAZ and the unaffected substrate were about 482 HV, 272 HV and 223 HV, respectively. As compared to the unaffected substrate, the microhardness in the HAZ was increased since during laser cladding the originally annealed microstructure has been re-austenitized and subsequently self-quenched into martensite. After annealing at 700 °C for 2 h, the respective microhardness of the clad, the HAZ and the unaffected substrate were changed to about 518 HV, 206 HV and 204 HV, respectively. Obviously, the difference in the microhardness between the HAZ and the unaffected substrate completely disappeared since the martensitic HAZ has been restored to the near equilibrium phases.

Figure 8 depicts the residual stresses in the Stellite 6 clad. The "as-clad" Stellite 6 shows relatively higher biaxial tensile stresses, with σ_L and σ_T being about 680 and 716 MPa, respectively. In contrast to the last case, the σ_L was slightly lower than the σ_T, and the same pattern was maintained throughout the post-cladding heat treatments. Annealing at temperature below 650 °C for 2 h gradually reduced the magnitudes of the stresses in the clad, while annealing at higher temperature above 700 °C for 2 h could reverse the sign of the stresses in the clad. The stresses (σ_L and σ_T) were reduced to 141 and 173 MPa after annealing at 650 °C for 2 h; they became compressive

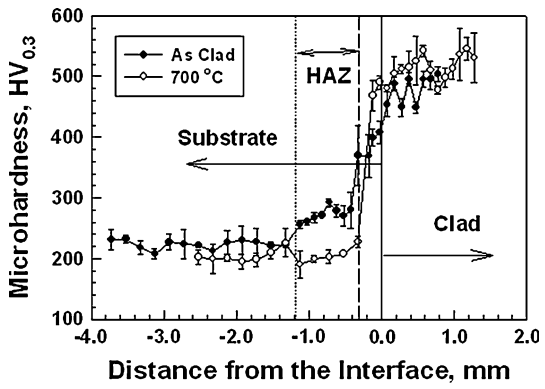

Fig. 7 Depth profiles of microhardness of laser-clad Stellite 6 on ASTM Class "C" wheel steel in "as-clad" and "after annealed at 700 °C for 2 h" conditions

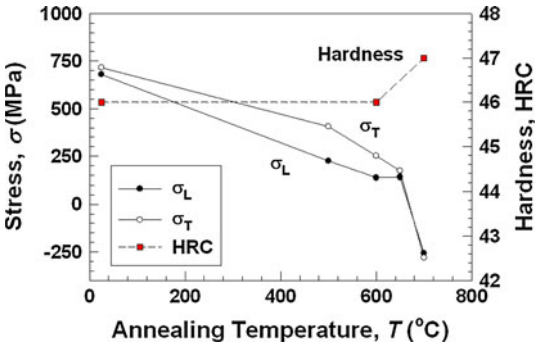

Fig. 8 The residual stress (σ) and hardness in Stellite 6 clad versus annealing temperature, in which the "L" and "T" represent the stress parallel to and transverse to the laser cladding direction, respectively

(with σ_L and σ_T being about −257 and −281 MPa, respectively) after annealing at 700 °C for 2 h, with an accompany of an insignificant increase in the hardness.

In contrast to the laser-clad IN-625 on IN-625 substrate, Stellite 6 clad was paired with a dissimilar substrate of Class "C" wheel steel. The nominal CTE of Stellite 6 alloy from 28 to 1000 °C is 17.5 × 10^{-6}/K on average [29], whilst that of Class "C" wheel steel (chemically similar to AISI 1075 carbon steel) is assumed as 13.6 × 10^{-6}/K between 0 and 400 °C (by averaging the CTEs of AISI 1070 and 1080 carbon steels in ferritic state [35]) and as about 23.1 × 10^{-6}/K in austenitic state at high-temperature (based on the CTE curve for Fe–C alloys [44]). During cladding, when the heat was conducted into the substrate, rising the temperature of the HAZ (Class "C" wheel steel) to above its A_{c1} led to the formation of austenitic phase (γ). Figure 9a schematically represents the clad, the austenitic HAZ, and unaffected substrate at solidification temperature of the clad in a state free of stress and deformation. Afterward, with rapid cooling, the clad and austenitic HAZ were thermally contracted if not impeded (Fig. 9b); in fact, internal stresses raised, as thermal contraction of both clad and austenitic HAZ was impeded by the unaffected substrate (similar to the previous case). In addition, the austenitic HAZ should contract more (owing to a larger CTE) than the Stellite 6 clad at this stage, which would cause certain mismatch between them, generating a local stress gradient at the interface. In general, accumulated tensile stresses in the clad and HAZ should be in tension, subjected to certain high-temperature relaxation because of their low yield strengths.

However, when the temperature rapidly dropped to below the martensitic start temperature, M_s, of the HAZ (roughly 274 °C or less [45]), a martensitic transformation occurred in the HAZ, causing a progressive volumetric increase during continued cooling until approaching to the martensitic finish temperature, M_f (roughly 149 °C or lower [45]) (Fig. 9c). A high compressive effect in the HAZ can readily build-up due to the high yield strength of

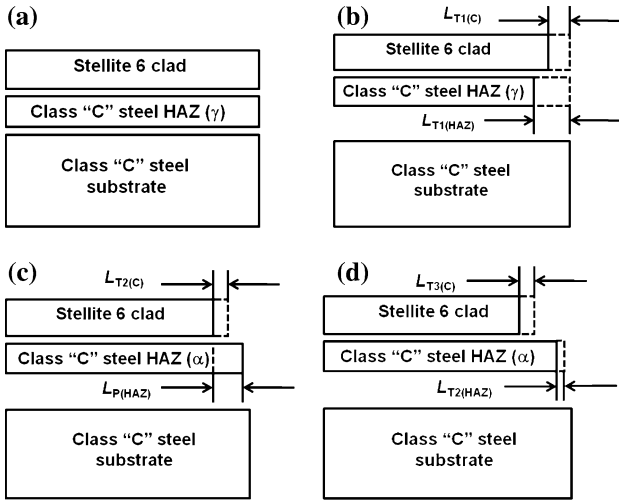

Fig. 9 Schematic of overall deformations (L) of the Stellite 6 clad, the HAZ and the unaffected substrate during cooling, if not impeded: **a** at solidification temperature of the clad, **b** above the M_s of the HAZ, **c** between the M_s and the M_f of the HAZ and **d** between the M_f of the HAZ to the ambient temperature, where the subscripts "T" and "P" refer to thermal- and phase-transformation-induced, whereas the subscripts "C" and "HAZ" represent clad and heat-affected zone, respectively

the HAZ at that relatively low temperature range if the volumetric dilation of the HAZ was impeded, which reduced the existing tensile stresses in the HAZ or even probably caused a sign reversal to the stresses. For the reason of equilibrium, this effect could adversely lead to more tensile stresses in the clad. Additionally, the impeded thermal contraction in the clad continued to add more tensile stresses inside itself. In general, the presence of martensitic transformation in the HAZ plays an adverse role through amplifying the magnitudes of tensile stresses in the Stellite 6 clad [14]. Bendeich et al. [46] have observed such a phenomenon, as the same as discussed above, in laser-clad Stellite 6 onto martensitic SS420 substrate through neutron diffraction measurement.

After the M_f of the substrate, both Stellite 6 clad and martensitic HAZ would continue to cool down to the ambient temperature and generate further thermal contraction, in which the clad contracted more than the HAZ (Fig. 9d). This could exert additional tensile effect on the resulting stresses in the clad if impeded [47].

In order to reduce the residual stresses in the clad, a pre-heating of the substrate during cladding is preferable. In an ideal condition, the pre-heating process has to ensure that no martensitic transformation occurs in the austenitic HAZ since the latter tends to produce more tensile stresses (as discussed above) in the clad due to the required mechanical balance [14].

During post-cladding annealing, with increasing temperature, the clad could gain some stress relaxation from its own plastic deformation or creep induced by low yield

strength at high temperature, as the nominal hot hardness of Stellite 6 material, a reflection of the ability to resist deformation at high temperature, can drop significantly (from 410 DPH at 20 °C to 301 DPH at 500 °C, 235 DPH 600 °C and 138 DPH at 800 °C, respectively, as reported in [29]). Most importantly, the martensitic HAZ was gradually decomposed into relatively equilibrium phases, resulting in an overall volume contraction which could induce a significant "compressive" effect on the clad. This brought a potential reduction or even a sign reversal to the existing tensile stresses in the clad. In the present case, the biaxial tension in the clad gradually decreased at annealing temperature below 650 °C and abnormally reversed into the compressive stresses after annealing above 700 °C for 2 h (Fig. 8).

Laser-clad CPM 10V tool steel onto AISI 1070 carbon steel

It is well known that laser cladding could present a complex and heterogeneous microstructure and properties that differ from point to point [48–50], since cladding is performed through a partial overlap of clad tracks to cover desired area on the surface of a substrate, that is, when a new clad track is deposited, a portion of the previously deposited neighbouring clad track is re-melted and solidified together with the injected powder to form the new clad track; while the microstructure in the previously deposited clad track adjacent to the re-melting area is thermally affected. For laser-clad IN-625 and Stellite 6 alloys, the mentioned phenomenon was not so significant; however, for the steels, these local thermal cycles could activate solid-state phase transformations that lead to progressive modification of microstructures and properties of previously deposited clad tracks such as martensite tempering, partial or total austenitization as well as transformation of austenite into martensite [48]. Thereby, two distinct but adjacent zones alternatively exist in the "as-clad" clad: "as-deposited" and "re-heated" zones. More accurately, the "re-heated" zone could be divided into two regions: (1) a "re-austenitized" region in which, as the re-heating temperature exceeds A_{c1}, martensitic phase in that region would transform into austenite (which would transform into martensite again upon subsequent rapid cooling), and the carbides would progressively be dissolved; and (2) a "tempered" region where since the re-heating could only reach to the temperature lower than A_{c1}, certain level of tempering in that region might occur [48–50]. Figure 10 schematically depicts the morphological relationship of "as-deposited" zone, "re-austenitized" and "tempered" regions. For the laser-clad CPM 10V tool steel, the morphological difference of the "as-deposited" and the "re-austenitized" was significant (see Fig. 11a) while it

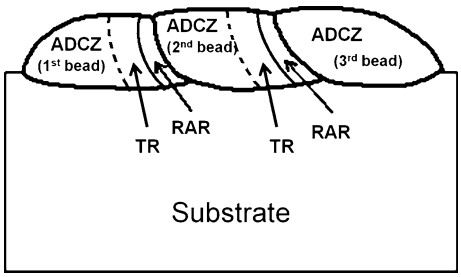

Fig. 10 Schematic of a cross-sectioned view of multiple overlapped CPM 10V clad beads (tracks), showing the areas of "as-deposited clad zone" (ADCZ), "re-austenitized region" (RAR) and "tempered region" (TR)

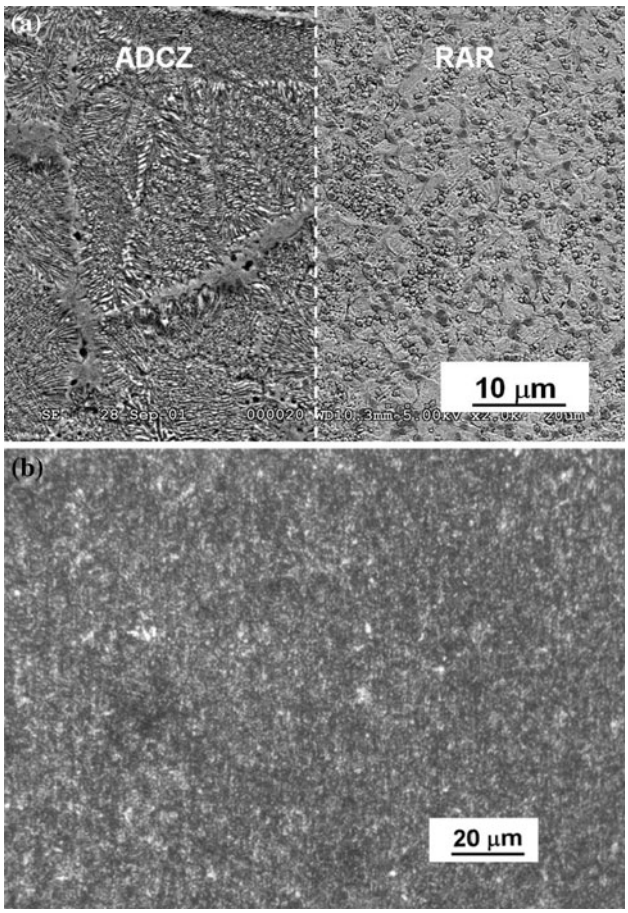

Fig. 11 Microstructures of laser-clad CPM 10V on AISI 1070 in "as-clad" condition: **a** at "as-deposited clad zone" (ADCZ) and "re-austenitized region" (RAR) of the clad and **b** in "heat-affected zone" (HAZ) of the substrate, respectively

was hard to differentiate the "as-deposited" with the "tempered" since the highly alloyed CPM 10V tool steel has a high resistance to tempering (which normally needs double or triple tempering at 550 °C for 2–3 h [31]). Hence, under the circumstance of rapid heating and cooling, tempering caused by thermal cycles during cladding may not be effective, even thought the chemical etched

morphology of the "as-clad" clad has shown some non-uniform narrow grey band areas, indicating the presence of tempered martensite in the "tempered" regions after cladding.

The SEM microstructure of the "as-deposited" zone looks like lamellar-like eutectic microstructure along with primary carbides at the grain boundaries, while that of the "re-austenitized" region shows fine globular carbides evenly distributed in the matrix with some martensitic characteristics [51]. The XRD pattern (Fig. 12) reveals that, in "as-clad" condition, the CPM 10V clad was dominated by retained austenite (γ'), martensite (α) and primary vanadium carbide (VC). Recently, Leunda et al. [52] observed the similar morphological characteristics in laser-clad CPM 10V tool steel produced using CW Nd:YAG laser as well. Moreover, Kury et al. [53, 54], having investigated rapidly solidified gas-atomized powder of highly alloyed V–Cr tool steel (3%C–3%Cr–12%V), noted that morphological variants of carbides in tool steels of ledeburite type are closely related to complicated thermal condition during solidification. A deep discussion on how the morphology of the carbides in the laser-clad CPM 10V tool steel evolved, therefore, is beyond the scope of this study. As compared with its prior annealed microstructure, the HAZ (1070 carbon steel) with a thickness of about 1.3 mm shows martensitic characteristics (Fig. 11b) due to re-austenitization and self-quenching during cladding.

Comparatively, after tempering at 260–600 °C for 2 h, the lamellar-like eutectic microstructure in the "as-deposited" zone in the CPM 10V clad still remained intact whereas the globular carbides in the "re-austenitized" region became slightly coarse (Fig. 13a). The XRD patterns (Fig. 12) reveal that when tempering at 260 °C for 2 h, the amount of the retained austenite had no significant change; while after tempering at 600 °C for 2 h, the retained austenite was substantially decreased to near zero. Meanwhile, the martensitic HAZ was highly tempered (Fig. 13b).

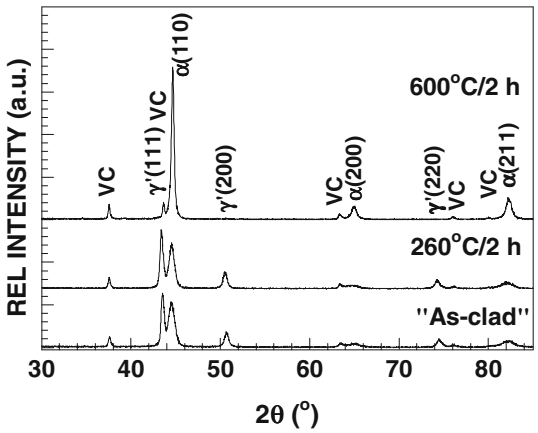

Fig. 12 XRD patterns of laser-clad CPM 10V on AISI 1070 carbon steel in "as-clad", "after tempered at 260 °C for 2 h" and "after tempered at 600 °C for 2 h" conditions

Figure 14 depicts the depth profiles of microhardness in the laser-clad CPM 10V tool steel in both "as-clad" and "after tempered at 600 °C for 2 h" conditions. The

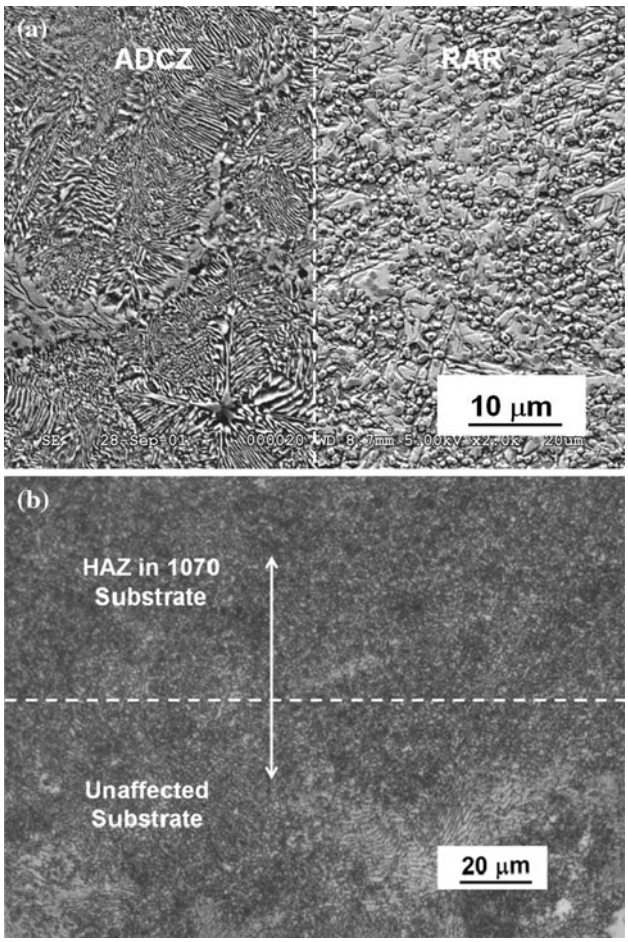

Fig. 13 Microstructures of laser-clad CPM 10V on AISI 1070 in "after tempered at 600 °C for 2 h" condition: **a** at "as-deposited clad zone" (ADCZ) and "re-austenitized region" (RAR) and **b** in "heat-affected zone" (HAZ) and unaffected substrate, respectively

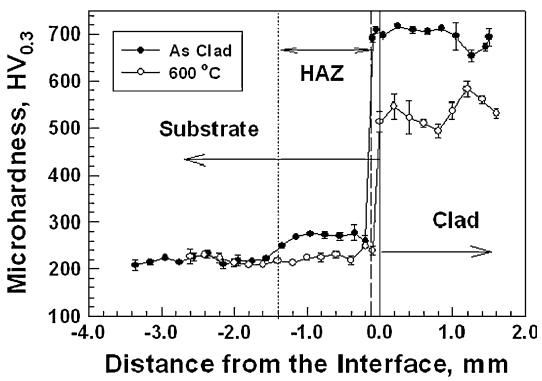

Fig. 14 Depth profiles of microhardness of laser-clad CPM 10V on AISI 1070 in "as-clad" and "after tempered at 600 °C for 2 h" conditions

thickness of the penetration (or dilution) layer was about 0.1 mm. In "as-clad" condition, the average microhardness of the clad, the HAZ and the unaffected substrate were about 696 HV, 271 HV and 219 HV, respectively. As compared with the unaffected substrate, the increased hardness in the HAZ reflected a phase change from the original hypoeutectoid to the resulting martensite during cladding. Furthermore, after tempering at 600 °C for 2 h, the respective microhardness of the clad, the HAZ and the unaffected substrate were about 533 HV, 233 HV and 218 HV, respectively. Both clad and HAZ showed a tempering-induced decrease in their microhardness.

Figure 15 shows the residual stresses in the CPM 10V clad as a function of tempering temperature. The "as-clad" CPM 10V shows relatively low tensile stresses (σ_L and σ_T) in the clad: about 135 and 100 MPa. The magnitudes of the residual stresses in the clad were reduced after tempering at relatively low temperature, while their signs could be reversed from the tension to the compression after tempering at high temperature. For instance, after tempering at 260 °C for 2 h, the magnitudes of stresses in the clad were reduced by about 26%; after tempering at 600 °C for 2 h, the resultant stresses (σ_L and σ_T) switched to about −128 and −144 MPa.

In contrast to the laser-clad IN-625 onto IN-625 and Stellite 6 onto Class "C" steel, for laser-clad CPM 10V tool steel onto AISI 1070 carbon steel, solid-state phase transformations in both clad and HAZ could yield additional contributions to the development of stresses during cooling, in addition to thermal shrinkage. Due to the complexity of microstructural evolution related to laser cladding of steels [48–50, 55–58], which involves melting, solidification, transformation of austenite into martensite, martensite tempering, and partial or total re-austenitization, depending on local thermal cycles of the clad, for understanding the build-up of residual stresses in a simple and straightforward way, one could consider primarily of the solidification, cooling down and martensitic transformation

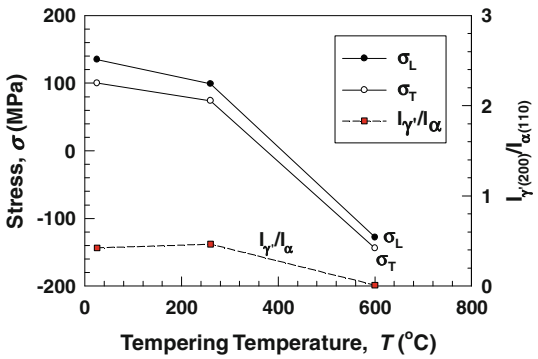

Fig. 15 The residual stress (σ) and retained austenite (γ') in CPM 10V clad versus tempering temperature, in which the "L" and "T" denote the direction parallel to and transverse to the laser cladding direction, respectively

of a single CPM 10V clad track, and re-visit any additional factors brought by "re-heating" during the deposition of multiple clad tracks/layers since the "re-heating" normally affected only a small portion of previous clad and merely modified, progressively, the percentage of phases such as martensite and austenite.

The presence and origin of primary ferritic δ or austenitic γ phase during the solidification of steel depend on the chemical composition, mainly on its carbon content, and thermal condition. For carbon content higher than roughly 1.3%, the primary phase is γ [55]. Moreover, the growth kinetics of γ phase is more favourable at higher solidification rate such as laser processing [56, 57]. Hence, when a laser beam created a CPM 10V melt with a carbon content of about 2.45%, it was reasonably assumed that the dominated phase in the solidified melt was austenitic phase (γ) along with a large amount of primary vanadium carbides (VC). Simultaneously, the substrate under the melt was thermally affected and re-austenitized to form HAZ. In this stage, due to their low yield strengths, it was assumed that the lengths of the clad and the HAZ were equal to the rest of the substrate, which meant a stress-free state at solidification temperature of the clad (Fig. 16a). If assuming that the CTE of CPM 10V in the state of austenite is lower than that of austenitic 1070 steel (which should be reasonable, considering the fact that the nominal CTE of CPM 10V tool steel from 21 to 593 °C in the state of ferrite is 12.3×10^{-6}/K [31] and that of 1070 steel in the state of ferrite is estimated to be 14.0×10^{-6}/K between 0 and 400 °C [35]), this difference of the CTEs between the clad and the austenitic HAZ could result in a thermal mismatch during continued cooling before reaching to their M_ss, and the clad contracted slightly less than the HAZ if no constraint was applied (Fig. 16b). Similar to the laser-clad IN-625 onto IN-625 and Stellite 6 onto Class "C" wheel steel, tensile stresses were expected to form in the clad and HAZ if impeded by the unaffected substrate. Likewise, at relatively high temperature (above their M_ss), thermal relaxation in both austenitic CPM 10V and 1070 prevented residual stresses, after built up, from being increased to a high level.

The martensitic transformation could start as soon as the temperature drops below the M_s. However, due to rapid solidification and high cooling rate, several factors would affect the ups and downs of the M_s of steels: rapid cooling rate and high dislocation density raised the M_s, whereas supersaturation of austenite in alloying elements, residual tensile stresses and refined austenite grain size (if less than 50 μm) decreased the M_s [56, 57]. Colaço and Vilar had studied the stabilization of austenite in tool steel induced by laser surface re-melting and found that in some cases, austenite could be fully retained at ambient temperature if the M_s was depressed to below 0 °C [56, 57]. For the

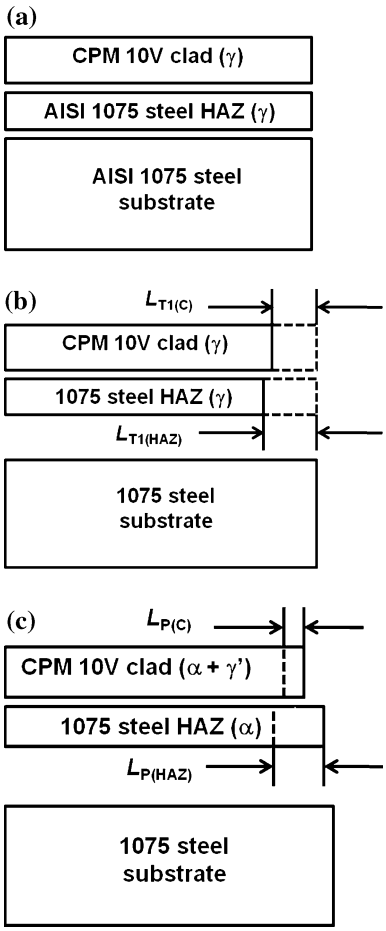

Fig. 16 Schematic of overall deformations (L) of the CPM 10V clad, the HAZ and the unaffected substrate, if not impeded: **a** at solidification temperature of the clad, **b** above both M_ss, **c** between both M_ss to pre-heating temperature of the substrate (150–200 °C), where the subscripts "T" and "P" refer to thermal- and phase-transformation-induced, respectively, whereas the subscripts "C" and "HAZ" represent clad and heat-affected zone, respectively

laser-clad CPM 10V, nevertheless, the martensitic transformation indeed happened during the period of rapid cooling in spite of the presence of a pre-heated substrate (150–200 °C) since, as previously mentioned that, the "as-clad" clad has shown the presence of non-uniformly distributed tempered martensite. Hence, it could be assumed that the M_s of the CPM 10V clad was higher than 200 °C.

Thereafter, the martensitic transformations would occur in both austenitic clad and HAZ, when the temperature dropped to below both M_ss (higher than 200 °C), introducing a progressive volumetric expansion with increasing undercooling (Fig. 16c). For the HAZ (1070 carbon steel), its M_f was roughly 149 °C [45]; whilst for most of tool steels such as CPM 10V, because of the stabilization of austenite [56, 57], their martensitic transformation could not complete even after cooling down to ambient temperature (M_f was normally below 0 °C) [59] and consequently, a large amount of austenite would retain in the clad when the clad specimen reached to the pre-heating temperature of the substrate where the martensitic transformation for the 1070 carbon steel was almost complete. Hence, the volumetric dilation effect caused by the martensitic transformation was far more significant in the HAZ than in the clad. This may partly or fully counteract their thermal contractions.

After the first clad track was deposited, the newly deposited steel clad presented a microstructure consisting of martensite, retained austenite and vanadium carbide. With the continued deposition of new clad tracks/layers, multiple re-heating could activate solid-state phase transformations (such as tempering, re-austenitizing and re-quenching) that led to progressive modification of overall percentage of phases in the clad [48–50]. Additionally, after the completion of cladding, the whole clad specimen would cool down from pre-heated substrate temperature to ambient temperature, resulting in further martensitic transformation in the clad, and introduced additional compressive effect on the clad, reducing overall level of tensile stresses inside itself. The experiment has shown that although the resultant stresses in the CPM 10V clad were still tensile, the magnitudes of the stresses were relatively low.

Since the "as-clad" CPM 10V tool steel still retained a certain amount of austenite, which provided an additional room to reduce or even reverse the tensile stresses in the clad through post-tempering. Consequently, with increased tempering temperature, the amount of retained austenite in the clad was gradually transformed into tempered martensite, resulting in a decrease in the tensile stresses in the clad due to related volumetric dilation. At the end, after tempering at about 600 °C for 2 h, the stresses in the clad were reversed from biaxial tension to compression with a near zero amount of retained austenite inside the clad (Fig. 15).

Concluding remarks

The selected nickel-based IN-625 superalloy, cobalt-based hardfacing Stellite 6 alloy and high-vanadium CPM 10V tool steel in powder forms have been successfully laser cladded, with/without pre-heating, on wrought IN-625 alloy, ASTM Class "C" wheel steel and AISI 1070 carbon steel substrate, respectively. The clads so obtained were metallurgically sound and dense with no crack and a few pores. Laser cladding induced residual stresses in the clad were closely correlated with thermal contraction and with the microstructural evolution in both clad and HAZ during cladding. Post-cladding heat treatments also exerted significant influences on the stress state in the clad. The investigation of combined effect of the clad and the HAZ on the residual stresses allows the following conclusions to be drawn:

(1) If applicable, both thermal contraction and solid-state phase transformations in the clad and HAZ during cooling play crucial roles in the development and controllability of process-induced residual stresses in the clad.
(2) In the case of no solid-state phase transformation during cladding and post-cladding heat treatments, e.g., for laser-clad IN-625 on wrought IN-625, the tensile stresses in the clad are normally generated by the constrained thermal deformation in the clad and HAZ. Annealing at high temperature could alleviate the intensities of residual stresses through thermal relaxation.
(3) In the case of laser-clad Stellite 6 on Class "C" wheel steel, where there are solid-state phase transformations in the HAZ, thermal deformation in the clad and HAZ as well as the phase transformations in the HAZ will play significant roles both during cladding and at the stage of post-cladding tempering.
(4) In the case of laser-clad CPM 10V on 1070 steel substrate, where there are solid-state phase transformations in both clad and HAZ during both cladding and post-cladding heat treatment, the phase transformations in both clad and HAZ could significantly affect the resultant distribution of residual stresses in the clad, in addition to thermal contraction.

Acknowledgements Authors would like to thank J. Fenner, A. Chen and M. Meinert (NRC-IMI-London) for their important contributions on the preparation and metallurgical characterization of the clad specimens. Authors highly appreciated critical comments and suggestions from the paper's reviewers as well, which were beneficial to the improvement of discussion in this article.

References

1. Jensen TA (2001) In: Ready JF, Farson DF (eds) LIA handbook of laser materials processing. LIA/Magnolia Publishing Inc., Orlando, p 284
2. Steen WM (1998) Laser material processing, 2nd edn. Springer, London, p 248
3. Vilar R (1999) J Laser Appl 11(2):64
4. Toyserkani E, Khajepour A, Corbin S (2005) Laser cladding. CRC Press, Boca Raton, p 1
5. Schubert E, Seefeld T, Rinn A, Sepold G (1999) J Therm Spray Technol 8(4):590
6. Dubourg L, Archambeault J (2008) Surf Coat Technol 202:5863
7. Sliva B, Pires I, Quintino L (2008) Mater Sci Forum 587–588:936
8. Xu G, Kutsuna M, Liu Z, Yamada K (2006) Surf Coat Technol 201:1138
9. Thompson S (1999) Handbook of mold, tool and die repair welding. William Andrew Publishing, Burlington, p 3
10. Preciado WT, Bohorquez CEN (2006) J Mater Process Technol 179:244
11. Champagne VK (2007) In: Champagne VK (ed) The cold spray materials deposition process: fundamentals & applications. Woodhead Publishing Limited, Cambridge, England, p 327
12. Gnyusov SN, Gnyusov KS, Durakov VG (2008) Weld Int 22(12):863
13. Bruckner F, Lepski D, Beyer E (2007) J Therm Spray Technol 16(3):355
14. Lepski D, Bruckner F (2009) In: Dowden J (ed) The theory of laser materials processing: heat and mass transfer in modern technology. Springer, The Netherland, p 235
15. Chen JY, Xue L, Visscher H, Wolfe J (2009) In: Symposium on surface protection for enhanced material performance in materials science & technology 2009 (MS&T'09), Pittsburgh, p 2090
16. Dekumbis R (1989) In: Proceedings of 6th conference on lasers in manufacturing, Birmingham, UK, IFS Ltd, p 185
17. Pei YT, De Hosson JThM (2000) JOM-e 52(1). http://www.tms.org/pubs/journals/JOM/0001/Pei/Pei-0001.html
18. Inoue T (2005) In: Feng Z (ed) Processes and mechanisms of welding residual stress and distortion. Woodhead Publishing Ltd., Cambridge, England, p 100
19. Inoue T (2002) In: Totten G, Howes M, Inoue T (eds) Handbook of residual stresses and deformation of steel. ASM International, Materials Park, p 296
20. Pilloz M, Pelletier JM, Vannes AB (1992) J Mater Sci 27:1240. doi:10.1007/BF01142030
21. Dubourg L, Hlawka F, Cornet A (2006) In: Sudarshan TS, Jeandin M, Stiglich JJ (eds) Surface modification technologies XVIII. ASM International, Materials Park, p 331
22. Chen Y, Liang X, Liu Y, Xu B (2010) Mater Des 31:3852
23. Pluyette E, Sprauel JM (1994) In: Proceedings of 4th international conference on residual stresses, Baltimore, Maryland, p 860
24. Grum J, Znidarsic M (2002) Mater Sci Forum 404-407:437
25. Tuominen J, Vuoristo P, Mantyla T (2005) In: ICALEO 2005, LIA, p 635
26. De Oliveira U, Ocelik V, De Hosson JThM (2006) Surf Coat Technol 201:533
27. De Freitas M, Pereira MS, Michaud H, Pantelis D (1993) Mater Sci Eng A 167:115
28. Sexton L, Lavin S, Byrne G, Kennedy A (2002) J Mater Process Technol 122:63
29. Deloro Stellite, Stellite® 6 Alloy (Technical Data). www.stellite.com
30. Frenk A, Henchoz N, Kurz W (1993) Z Metallkd 84(12):886
31. Crucible Research Service Centre (2003) CRUCIBLE CPM® 10 V® (AISI A11), Issue #7
32. Hu YP, Chen CW, Mukherjee K (1998) J Mater Sci 33:1287. doi:10.1023/A:1004346214050
33. Donachie MJ, Donachie SJ (eds) (2002) In: Superalloys: a technical guide. ASM International, Materials Park, p 4
34. ASTM International (2009) Standard specification for wrought carbon steel wheels (Designation: A 504/A 504M–08)
35. Bauccio M (ed) (1993) In: ASM metals reference book, 3rd edn. ASM International, Materials Park, p 302
36. Donachie MJ, Donachie SJ (eds) (2002) In: Superalloys: a technical guide, 2nd edn. ASM International, Materials Park, p 245
37. Xue L, Theriault A, Chen JY, Islam MU, Wieczorek A, Draper G (2002) In: Srivatsan TS, Varin RA (eds) Processing & fabrication of advanced materials X. ASM International, Materials Park, p 361
38. Measurements Group, Inc. (1992) Model RS-200 milling guide—instruction manual
39. Lu J, James MR, Mordfin L (1997) In: Lu J (ed) Handbook of measurement of residual stresses. The Fairmont Press, Inc., Lilburn, p 229
40. Conlon K, Rogge R, Chen JY, Xue L (2005) Investigation of residual stresses in laser-clad metal plates by neutron diffraction, NRC-SIMS Internal Report

41. Haynes international, high-temperature alloys data sheet H-3073D: Haynes 625 alloy. http://www.haynesintl.com
42. D'Oliveira ASCM, Da Silva PSCP, Vilar R (2002) Surf Coat Technol 153:203
43. Chang SS, Wu HC, Chen C (2008) Mater Manuf Process 23:708
44. Onink M, Brakman CM, Tichelaar FD, Mettemeijer EJ, Van der Zwaag S, Root JH, Konyer NB (1993) Scripta Metall Mater 29:1011
45. Blackwood RR, Jarvis LM, Hoffman DG, Totten GE (1998) In: The 18th ASM heat treating society conference & exposition, Rosemont, IL, p 575
46. Bendeich P, Alam N, Brandt M, Carr D, Short K, Blevins R, Curfs C, Kirstein O, Atkinson G, Holden T, Rogge R (2006) Mater Sci Eng A 437:70
47. Zinn W, Scholtes B (2002) In: Totten GE, Howes M, Inoue T (eds) Handbook of residual stresses and deformation of steel. ASM International, Materials Park, p 391
48. Costa L, Vilar R, Reti T, Colaço R, Deus AM, Felde I (2005) Mater Sci Forum 473–474:315
49. Costa L, Reti T, Deus AM, Vilar R (2002) In: Keicher D, Sears JW, Smugeresky JE (eds) Proceedings of international conference on metal powder deposition for rapid manufacturing, MPIF, Princeton, NJ, p 172
50. Vilar R, Colaço R, Almeida A (1995) Opt Quant Electron 27:1273
51. Wang SH, Chen JY, Xue L (2006) Surf Coat Technol 200:3446
52. Leunda J, Soriano C, Sanz C, García Navas V (2011) Physics Procedia 12:345
53. Kusy M, Caplovic L, Grgac P, Vyrostkova A (2004) J Mater Process Technol 157–158:729
54. Kusy M, Grgac P, Behulova M, Vyrostkova A, Miglierini M (2004) Mater Sci Eng A 375–377:599
55. Boccalini M, Goldenstein H (2001) Int Mater Rev 46(2):92
56. Colaço R, Vilar R (1998) J Mater Sci Lett 17:563
57. Colaço R, Vilar R (2004) Mater Sci Eng A 385:123
58. Hemmati I, Ocelík V, De Hosson JThM (2011) J Mater Sci 46:3405. doi:10.1007/s10853-010-5229-2
59. Linde group, white paper: sub-zero treatment: technology, processes and equipment, 1st Sept. 2010, Germany. www.linde-gas.com